Higher Metal−Ligand Coordination in the Catalytic Site of Cobalt-Substituted *Thermoanaerobacter brockii* Alcohol Dehydrogenase Lowers the Barrier for Enzyme Catalysis[†]

Oded Kleifeld,[‡] Lubomír Rulíšek,[§] Oren Bogin,[||] Anatoly Frenkel,[⊥] Zdeněk Havlas,[§] Yigal Burstein,[||] and Irit Sagi*,[‡]

Department of Structural Biology, The Weizmann Institute for Science, Rehovot 76100, Israel, Institute of Organic Chemistry and Biochemistry, Academy of Sciences of the Czech Republic, and Center for Complex Molecular Systems and Biomolecules, Flemigovo náměstí, 2, 166 10 Prague 6, Czech Republic, Department of Organic Chemistry, The Weizmann Institute for Science, Rehovot 76100, Israel, and Department of Physics, Yeshiva University, New York, New York 10016

ABSTRACT: *Thermoanaerobacter brockii* alcohol dehydrogenase (TbADH) is a zinc-dependent NADP$^+$/H-linked class enzyme that reversibly catalyzes the oxidation of secondary alcohols to their corresponding ketones. Cobalt substitution studies of other members of the alcohol dehydrogenase (ADH) family showed that the cobalt-containing ADHs have a similar active site structure but slightly decreased activity compared to wild-type zinc ADHs. In contrast, the cobalt-substituted TbADH (Co-TbADH) exhibits an increase in specific activity compared to the native enzyme [Bogin, O., Peretz, M., and Burstein, Y. (1997) *Protein Sci. 6*, 450−458]. However, the structural basis underlying this behavior is not yet clear. To shed more light on this issue, we studied the local structure and electronics at the catalytic metal site in Co-TbADH by combining X-ray absorption (XAS) and quantum chemical calculations. Importantly, we show that the first metal−ligand coordination shell of Co-TbADH is distorted compared to its native tetrahedral coordination shell and forms an octahedral structure. This is mediated presumably by the addition of two water molecules and results in more positively charged catalytic metal ions. Recently, we have shown that the metal−ligand coordination number of the zinc ion in TbADH changes dynamically during substrate turnover. These structural changes are associated with a higher coordination number of the native catalytic zinc ion and the consequent buildup of a positive charge. Here we propose that the accumulation of a higher coordination number and positive charge at the catalytic metal ion in TbADH stabilizes the structure of the catalytic transition state and hence lowers the barrier for enzyme catalysis.

Alcohol dehydrogenases (ADHs)[1] constitute one of the most extensively studied families of metalloenzymes. These oxidoreductases catalyze the interconversion of alcohols, aldehydes, and ketones in various stages of metabolic pathways in both prokaryotes and eukaryotes. ADHs require either NAD$^+$(H) or NADP$^+$(H) as a cofactor for catalysis. Most ADHs contain zinc at the active site (*2*). Zinc-dependent ADHs are dimers, usually found in higher plants and mammals, or tetramers, such as those present in yeasts and bacteria.

For most members of the ADH family, the kinetics of the reaction with alcohols and aldehydes follow a Thorell−Chance sequential mechanism, where the binding of the cofactor is the first step and its dissociation is the last (and rate-determining) step (*3*, *4*). The oxidation of alcohols requires a net removal of two hydrogen atoms from the substrate. This dehydrogenation process is known to proceed by the coupled processes of proton abstraction and hydride ion transfer. Several catalytic mechanisms for ADHs have been proposed, based on accumulating structural and spectroscopic evidence gathered from the most studied enzyme, horse liver alcohol dehydrogenase (HLADH) (*5*, *6*). Two main classes of structural mechanisms, based on a proton relay system, have been proposed for HLADH; they differ specifically in the hypothesized coordination of the zinc ion during catalysis. One mechanism involves the displacement of the zinc-bound water by the alcohol substrate; consequently, the zinc ion remains tetrahedrally coordinated during catalysis (*7*, *8*). Alternatively, the substrate molecule is added to the tetrahedral zinc ion to form pentacoordinated zinc (*9*, *10*).

An interesting development in the field of ADHs occurred when the bacterial NADP$^+$/H-linked alcohol dehydrogenase was purified from cell extracts of *Thermoanaerobacter brockii* (TbADH) (*11*). This extreme thermophilic alcohol

* To whom correspondence should be addressed: Department of Structural Biology, The Weizmann Institute of Science, P.O. Box 26, Rehovot 76100, Israel. Telephone and fax: 972-8-9342130. E-mail: irit.sagi@weizmann.ac.il.

[‡] Department of Structural Biology, The Weizmann Institute for Science.

[§] Academy of Sciences of the Czech Republic and Center for Complex Molecular Systems and Biomolecules.

[||] Department of Organic Chemistry, The Weizmann Institute for Science.

[⊥] Yeshiva University.

[1] Abbreviations: TbADH, *T. brockii* alcohol dehydrogenase; ADH, alcohol dehydrogenase; Co-TbADH, cobalt-substituted TbADH; XAFS, X-ray absorption fine structure; EXAFS, extended X-ray absorption fine structure; XANES, X-ray absorption near-edge structure.

dehydrogenase has received much attention, since unlike the well-studied HALDH and other eukaryotic ADHs, it possesses unique properties that are invaluable for industrial use (*12*). Specifically, TbADH is remarkably stable up to 85 °C, exhibits a high tolerance for organic solvents, and shows broad specificity and high reactivity toward secondary alcohols and low reactivity toward primary alcohols (*11*).

TbADH is a tetramer comprising four identical subunits, each containing 352 amino acid residues, corresponding to a molecular mass of ~38000 Da per subunit (*13*). The overall three-dimensional structures of TbADH and its analogues, alcohol dehydrogenase from *Clostridium beijerinckii* (CbADH), were studied by X-ray crystallography (*14*). Structurally, the sequences of CbADH and TbADH are 75% identical, and they have similar three-dimensional structures. The crystal structure of apo-CbADH (cofactor-free) shows that the single zinc ion in the catalytic site is bound to Cys-37, His-59, Asp-150, and Glu-60. The structures of TbADH in its holo (cofactor bound) form and CbADH in its apo and holo forms reveal few differences compared to the structures of other ADHs which include the type of ligation around the catalytic zinc ion, the absence of a structural zinc ion, and the lack of the conserved "proton relay" pathway (*14*).

Previously, we determined the microenvironment of the zinc site in TbADH in various complexes that are relevant to substrate turnover. In the first stage, stable complexes of TbADH suitable for structural characterization were achieved by using the inhibitor dimethyl sulfoxide (DMSO) which mimics substrate–product binding (*15*). These studies indicated that the catalytic zinc ion in TbADH forms a penta-coordination complex upon binding to DMSO. In addition, the change in coordination resulted in the accumulation of a positive charge on the zinc ion. These studies were further extended to the dynamic structural characterization of the enzyme reaction with the substrate 2-propanol, using time-resolved freeze-quench X-ray absorption coupled with pre-steady-state kinetics (*16*). Importantly, we have demonstrated that the microenvironment of the zinc site in TbADH undergoes dynamic and rapid structural changes that are closely related to the enzyme kinetics and the reaction mechanism. Specifically, during substrate turnover, the native tetrahedral coordination of the catalytic zinc ion is altered and forms a pentacoordinated intermediate, which is accompanied by a buildup of a positive charge on the metal ion.

To provide further mechanistic insights regarding the nature of this phenomenon, we substituted the TbADH catalytic zinc ion for cobalt. Interestingly, cobalt-substituted TbADH exhibited a higher specific activity toward its native substrate, 2-propanol (*1*). One of the most common and effective tools for determining the structural basis of the catalytic properties in zinc enzymes is by substituting the spectroscopically silent zinc ion for analogous metals such as cobalt and cadmium ions (*17*). Cobalt substitutions have been used extensively for studying the reaction mechanism of ADHs (*10, 18–20*). The crystal structure of the cobalt-substituted HLADH shows that the tetrahedral coordination of the catalytic metal is preserved (*19*). It is important to note that the cobalt-substituted HLADH exhibits kinetic properties similar to but slightly lower than those of the

native Zn-HLADH. Specifically, the k_{cat} of cobalt-containing HLADH was ~0.9-fold lower than that of Zn-HLADH (*21, 22*). Other studies aimed at elucidating the possible difference between the different isozymes of human ADH showed that the coordination environment of the catalytic cobalt ions is strictly conserved in both class I ADH (HLADH) and class III human ADH (*23*). Interestingly, investigations of cobalt-substituted HLADH by variation of the pH of steady-state kinetics and electron paramagnetic resonance (EPR) demonstrated that the active site's metal ion in the ternary enzyme–cofactor–alcohol complex is pentacoordinated with a neutral water molecule as a fifth ligand (*10, 24*).

Here we report comparative studies of Co-TbADH using X-ray absorption (XAS) spectroscopy complemented by high-level quantum chemical calculations. We show that the cobalt(II) ion in the highly reactive catalytic site in Co-TbADH possesses octahedral coordination. We suggest that the deviation from the native tetrahedral coordination of the metal ion is directly correlated with the higher reactivity of the substituted enzyme.

EXPERIMENTAL PROCEDURES

Materials. All chemicals were of the highest purity grade and were obtained from Merck (Darmstadt, Germany), except when otherwise noted. Trisma base, phenylmethanesulfonyl fluoride (PMSF), β-nicotinamide adenine dinucleotide phosphate (potassium salt) (NADP$^+$), D,L-dithiothreitol (DTT), ampicillin, and benzamidine were purchased from Sigma (St. Louis, MO). DEAE-Sepharose and Red Sepharose CL-6B were purchased from Pharmacia (Uppsala, Sweden). Ethylenediaminetetraacetic acid (EDTA) and 2-butanol were obtained from Fluka Chemical AG (Buchs, Swizerland). The protein assay kit was from Bio-Rad Laboratories (Richmond, CA).

Expression and Purification of Recombinant TbADH. Recombinant TbADH was purified according to a modification of the procedure described by Bogin *et al.* (*1*). Briefly, plasmids containing the TbADH sequence were transformed into the *Escherichia coli* TG-1 strain. The TG-1 cells were grown aerobically for 16 h at 37 °C in 2YT medium with ampicillin (100 μg/mL). Pelleted cells were resuspended in 25 mM Tris-HCl, 0.1 mM DTT, 0.1 mM EDTA, 1 mM benzamidine, and 0.02% sodium azide (pH 7.3) (buffer A). Cells were disrupted for 5 min by pulsed sonication (Branson 450 sonifier) within ice, followed by centrifugation at 23000g for 15 min. The supernatant was heat-treated for 10 min at 65 °C and then centrifuged again at 23000g for 20 min. The supernatant was applied to a DEAE-Sepharose column (7 cm × 3 cm), pre-equilibrated with buffer A containing protease inhibitors at 4 °C, and then extensively washed with buffer A until no protein was eluted. The recombinant protein was eluted from the column with a solution of 0.1 M NaCl in buffer A and applied to a Red Sepharose CL-6B column (13 cm × 3 cm), which was pre-equilibrated with buffer A containing protease inhibitors at 4 °C. The recombinant protein was eluted from the Red Sepharose column with a 400 mL NaCl linear gradient (from 0.1 to 1 M). Active fractions were collected and concentrated by ultrafiltration, using Amicon YM-30 from Millipore (Bedford, MA). The concentrated protein solution was collected and dialyzed extensively against buffer A.

Cobalt Substitution. TbADH catalytic zinc was replaced with cobalt following the published procedures (*1*). In brief, the metal substitution was accomplished using serial extensive dialysis sections, including the following steps: chelation of TbADH catalytic zinc ion using 1,10-phenanthroline, removal of 1,10-phenanthroline from the TbADH solution, and, finally, introduction of cobalt (cobalt acetate) into metal-free TbADH. The Co-TbADH was analyzed for zinc and cobalt content using inductively coupled plasma atomic emission spectroscopy (ICP-AES). Co-TbADH contains one coablt atom per subunit, which is equivalent to the molar amount of zinc in the wild-type enzyme (*1*). Co-TbADH exhibits a pH dependence similar to that of wild-type TbADH, with maximum activity for 2-propanol oxidation within the pH range of 8.0−9.0 (data not shown).

Inductively Coupled Plasma Atomic Emission Spectroscopy (ICP-AES). The metal content in TbADH and Co-TbADH was analyzed by inductively coupled plasma atomic emission spectroscopy using an ICP-AES model "Spectroflame" from Spectro (Kleve, Germany). Zinc and cobalt content were determined, after extensive dialysis of protein samples, against three changes of 100 volumes of metal-free 25 mM HEPES-HCl and 100 mM NaCl (pH 8.3). Samples were digested in nitric acid, and the volume was adjusted to 6 mL. Portions of this solution were analyzed versus certified standards. The measurement was repeated three times using protein samples from different batches.

Protein Concentrations. Protein concentrations were determined by the Bradford assay (*25*), with bovine serum albumin as the standard.

Enzyme Activity Assay. The enzymatic activity of Zn-TbADH and Co-TbADH (assayed in the direction of alcohol oxidation) was measured at 40 °C by following the absorption increase at 340 nm ($\epsilon_{340} = 6.2$ mM^{-1} cm^{-1}) for the formation of NADPH from NADP$^+$. One unit of enzyme activity is defined as the amount of enzyme that catalyzes the formation of 1 μmol of NADPH per minute at the initial velocity under the above-mentioned conditions.

The enzymatic activity was measured and calculated using a Beckman DU-7500 spectrophotometer equipped with a Multicomponent/SCA/Kinetics Plus software package and thermostatatic water-circulating bath. The reaction mixtures contained a total volume of 1 mL in 0.15 M Tris-HCl buffer (pH 9.0) and 0.5 mM NADP$^+$. Co-TbADH measurements were performed using similar metal-free solutions, with the addition of cobalt acetate which produced a final concentration of 2 μM. The concentrations of 2-propanol and 2-butanol were 0.05, 0.1, 0.2, 0.5, 0.7, and 1.0 mM. The kinetic parameters were calculated by fitting the initial velocities to the hyperbola function using the nonlinear fit tool of Origin 6.1 (OriginLab Corp.).

Preparation of Samples for X-ray Absorption (XAS). Enzyme samples were extensively dialyzed against three changes of 100 volumes of metal-free 25 mM HEPES and 100 mM NaCl (pH 8.3). HEPES buffer was used to avoid drastic pH changes in the cryogenic temperature. The use of HEPES buffer did not affect the enzymatic activity of Zn-TbADH and Co-TbADH. The enzyme sample was concentrated to produce a final concentration of 1 mM (∼40 mg/mL) by ultrafiltration, using a Millipore Centricon-30 (Bedford, MA) apparatus. Protein samples were loaded into copper holders (10 mm × 5 mm × 0.5 mm) covered with

Mylar tape and were immediately frozen in liquid nitrogen. The frozen samples were mounted into a Displex closed-cycle helium cryostat, and the temperature of the samples was maintained at 30 K to minimize the thermal disorder in the XAS data.

Data Collection for XAS. XAS data collection was performed at the National Synchrotron Light Source (NSLS) at Brookhaven National Laboratory (BNL, Upton, NY). The XAS of Co-TbADH samples was collected at beam line X9B. The spectra were recorded at the cobalt K-edge in fluorescence geometry at a low temperature (30 K). The beam energy was defined using a flat Si (111) monochromator crystal. The incident beam intensity (I_0) was recorded using an ionization chamber. The fluorescence intensity was recorded using a 13-element Ge detector. The transmission signal from a cobalt foil was measured with a reference ion chamber, at the same time as fluorescence, for beam energy calibration purposes. Several scans of each sample were collected for a total of 1 000 000 counts across the edge. The samples were checked for burn marks after each scan, and the beam position on the sample was changed before each scan to minimize damage by radiation. The enzyme activity was checked after exposure to X-ray, and the enzyme was found to be fully active.

The XAS of the cobalt model component cobalt(III) acetylacetonate (Co-AcAc) was measured at Agere/UIUC beamline X16C. X-ray absorption coefficients of this sample were measured at room temperature in the fluorescence mode by using the ion chamber for the incident beam and the Stern−Heald detector for fluorescent beams. No differences in edge energy were observed between Co-AcAc and Co-TbADH.

Data Processing and Analysis. The average cobalt K-edge absorption coefficient $\mu(E)$, obtained after several independent XAS measurements for each sample, was aligned in absolute energy, using the reference cobalt metal foil XAS data as an absolute energy calibrant. Then, the absorption coefficient for different samples was shifted in X-ray energy, until the white-line energies were aligned at the same energy (7720 eV).

The pre-edge regions of the X-ray absorption spectra of Co-TbADH and Co-AcAc were analyzed using normalization of the edge jump, followed by subtraction of the background and edge region with a function composed of linear and arctangent components, as described previously (*26*). Calculation of the pre-edge 1s−3d peak area after the background was subtracted was obtained either by integration over a range of ∼8 eV or by fitting to a Gaussian function, both of which gave identical results. The entire pre-edge analysis was carried out using Origin 6.1 (OriginLab Corp.).

The smooth atomic background was removed using the AUTOBK program of the UWXAFS data analysis package (*27*), developed at the University of Washington (Seattle, WA). The same energy ($E_0 = 7720$ eV) was chosen for the purpose of removing the background as the origin of the photoelectron energy. The R space region for minimizing the signal below the first shell was kept between 0 and 1 Å. After the background had been removed, the useful k range in the resulting k^2 weighting factor [$\chi(k)$] is between 2 and 10−10.5 Å^{-1}. Initial model data for the fitting procedure were constructed by extracting the catalytic zinc site coordinates (with a radius of 5 Å) from the crystallographic

coordinates of CbADH, because of its better structure resolution over TbADH's crystal structure (*14*). Using the computer code FEFF7 (*28*, *29*), we calculated the theoretical photoelectron-scattering amplitudes and phase shifts after replacing the zinc with cobalt ion. Further refinement of the fits was achieved using the structure of aqua-thiourea-[(*N*,*N*-diacetato)semicarbazido-*N*,*O*,*O*′,*O*″]-cobalt(II) as a model (*30*). Total theoretical $\chi(k)$ was constructed by adding the most important partial $\chi(k)$, which contributes to the *r* range of interest.

The k^2 weighting factor and the Hanning window function, defined between 2 and 9.5–10.0 Å^{-1}, were used in Fourier transformations for all data sets. During the fitting procedure, the various parameters, including the corrections to the energy origin (ΔE_0), bond distances (ΔR), and mean square disorders of the distances, the Debye–Waller factors (σ^2), were varied until the best fit was achieved. The number of relevant independent data points (N_{idp}) in the data was calculated using eq 1 (*31*):

$$N_{idp} = \frac{2\Delta k \Delta r}{\pi} + 2 \qquad (1)$$

where Δk and Δr are the data ranges in *k* and *r* space, respectively. Equation 1 implies that the number of fit variables should be smaller than N_{idp}. To reduce the number of fit variables, we optimized and fixed the many-body factor S_0^2 at 0.8. The theoretical XAFS signal was fitted to the experimental data, using the nonlinear least-squares method implemented in FEFFIT (*27*) in *R* space, by Fourier transforming both theory and data. Data and theory were weighted by k^2 and multiplied by a Hanning window function in Fourier transforms.

Computational Details. All the calculations were performed with the Gaussian 98 program suite (*32*) within the framework of density functional theory. The three-parameter functional developed by Becke (*33*) has been employed (denoted B3LYP). The optimization of the molecular geometries was carried out using the 6-31G basis set for the first and second row atoms. This was further augmented by diffuse functions, the (*s*,2*p*,*d*) set for Co and Zn, *sp* functions for other heavy elements, and a single set of polarization functions: *f* for TMs and *d* for other heavy elements. Single-point energy calculations on the optimized geometries were carried out using the triple-ζ (TZ) basis set of Wachters and Hay (*34*, *35*) for Co and Zn and the standard 6-311G set for other elements (H, C, N, O, and S) (*36*). It was augmented by the same diffuse functions as 6-31G with further addition of s functions for hydrogens and the following sets of polarization functions: 2*fg* for TMs, 2*df* for other heavy atoms, and 2*pd* for hydrogens. The exponents of all diffuse and polarization functions were used as implemented in Gaussian 98, and the described basis sets have been approached via 6-31+G(d) and 6-311++G(2df,2pd) keywords.

The properties of cobalt(II) complexes have been calculated for the lowest-quartet spin state, which is the ground electronic state in both of the considered coordination geometries (octahedral and tetrahedral) and a set of ligands (RCOO$^-$, RS$^-$, H$_2$O, and imidazole), whereas cobalt(III) has been assumed to be in a singlet $(t_{2g})^6(e_g)^0$ electronic configuration, which should be the lowest electronic state of this

Table 1: Kinetic Constants of Alcohol Oxidation for Zn-TbADH and Co-TbADH[a]

	2-butanol		2-propanol	
kinetic constant	Zn-TbADH	Co-TbADH	Zn-TbADH	Co-TbADH
K_m(app) (mM)	0.19	0.18	0.19	0.17
k_{cat} (μmol min^{-1} mg^{-1})	50	64	42	53
k_{cat}/K_m (min^{-1})	259	355	225	311

[a] Kinetic constants were determined at 40 °C in 150 mM Tris-HCl buffer (pH 9.0) by varying the substrate while keeping the cofactor at a saturating concentration. Initial velocities were measured and calculated as described in Experimental Procedures. Errors for fitted parameters were in the range of 5–10%.

ion (*37*). The interaction (complexation) energies are calculated according to eq 2 (*38*):

$$E_{int}(M,X_1,...,X_n) = \\ E([MX_1,...,X_n]^{c+}) - E(Bq_M X_1,...,X_n) - \\ (E\{[M(H_2O)_n]^{c+}\} - E[Bq_M(H_2O)_n]) \quad (2)$$

RESULTS AND DISCUSSION

Kinetic Characterization of Co-TbADH. Initial velocity studies provided the kinetic constants for substrate turnover using 2-propanol and 2-butanol (Table 1). Substitution of the catalytic zinc ion in TbADH with the cobalt ion increased the turnover number by approximately 1.4-fold. The apparent K_m values are similar for both substrates. Changes in the enzymatic efficiency were mainly due to the k_{cat} values of Co-TbADH being higher than those of wild-type TbADH (Table 1). Taken together, these results show that unlike cobalt substitutions of other ADHs (*20*, *21*), Co-TbADH exhibits a catalytic efficiency (k_{cat}/K_m) that is greater than that of wild-type Zn-TbADH. These results are in agreement with previously reported data for Co-TbADH (*1*).

XAS Studies. To provide additional insights regarding the increase in the enzyme efficiency of the cobalt-substituted enzyme, we examined the local structure around the metal ion by X-ray absorption spectroscopy (XAS). XAS is a unique structural technique capable of providing bond lengths, coordination numbers, and electronic structures around a target atom. This structural information can be obtained with a precision of 0.01 Å. Spectral analysis at the near-absorption edge provides information about the metal's charge state and geometry, whereas the extended X-ray absorption fine structure (EXAFS) region above the absorption edge provides structural information, such as metal–ligand coordination numbers, atom types, and metal–ligand distances.

Pre-Edge Spectral Analysis. Figure 1a shows the X-ray absorption near-edge structure (XANES) spectra of Co-TbADH and cobalt(III) acetylacetonate (Co-AcAc). When the region near the X-ray absorption edge is scanned, the excitation of a core electron to a bound state, below the ionization threshold, is excited, revealing substantial chemical and structural information. K-edge absorption spectra of octahedral transition metal complexes containing empty 3d orbitals generally exhibit a low-intensity peak approximately 10 eV before the edge. These peaks have been assigned to symmetry-forbidden transitions of 1s core electrons to 3d empty states (*39*, *40*). The intensity of the 1s–3d transition
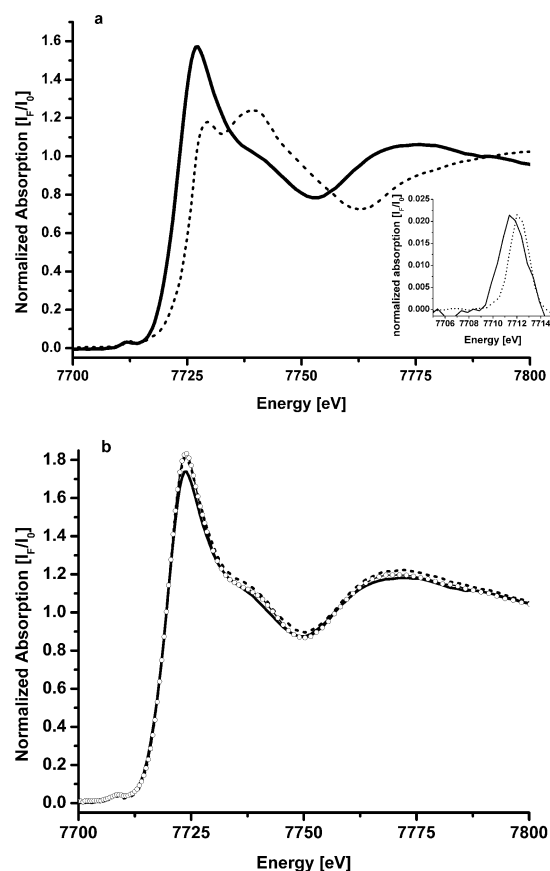
FIGURE 1: Comparison of raw, normalized XAS data in the cobalt K-edge region of (a) Co-TbADH (—) and cobalt(III) acetylacetonate (- - -). The insert shows a background-corrected pre-edge spectrum showing the 1s−3d transition. (b) Co-TbADH (—), the Co-TbADH−NADP$^+$ complex (- - -), and the Co-TbADH−NADP$^+$−DMSO ternary complex (○).

increases with a decrease in coordination number because of the loss of the inversion center in lower-symmetry complexes. The spectra of Co-TbADH and the octahedral Co-AcAc (*41*) compound contain similar small 1s−3d transitions at approximately 7711 eV. Integration of the 1s−3d intensities results in a peak area of 5.6×10^{-2} eV for Co-TbADH and 4.2×10^{-2} eV for Co-AcAc (Figure 1a inset). These values are consistent with octahedral cobalt sites (*39*). Overall, these results suggest that metal ion coordination in Co-TbADH is higher than the native coordination of the metal ion in Zn-TbADH (*14, 15*). In addition, we used the well-studied inhibitor DMSO (*8, 42*) to mimic binding of the substrate to the Co-TbADH active site. Inhibition of Co-TbADH with DMSO resulted in no significant change in the XANES spectrum (Figure 1b), in contrast to our previous studies of Zn-TbADH, which exhibited a distinct shift of ∼1.5 eV in the X-ray absorption edge position upon DMSO binding (*15*).

EXAFS Analysis. To obtain detailed information about the Co-TbADH active site structure, we conducted an EXAFS analysis of Co-TbADH and the Co-TbADH−NADP$^+$−DMSO complex. We used standard curve fitting procedures to fit the FEFF7 theory data to the real and imaginary parts of the Fourier-transformed $\chi(k)$ (*27−29*). The results of the EXAFS data analysis and the fitting parameters are presented in Table 2 and Figure 2.

The distances and coordination numbers obtained for the Co-TbADH samples were determined by analyzing each data set separately, avoiding the use of heavy constraints. The stability of the bond distance solutions derived for each structure was examined by varying the initial conditions of the distance and thermal disorder (Debye−Waller) parameters, while examining the contribution to the fit quality parameters, namely, χ^2 and *R*-factor values. The possibility of a higher coordination number (more than four ligands) at the active cobalt site was examined by either varying or fixing and stepping the coordination number, while testing the stability of the fitting results (Table 2). The values of ΔE_0 were optimized for each fit either by floating or by stepping analysis.

The local structure around the catalytic cobalt ion in the Co-TbADH enzyme, determined by our EXAFS data analysis procedures (Table 2), was best fitted to the octahedral model; it consists of one Co−O/N contribution at a bond distance of 1.86 ± 0.03 Å, four Co−O/N contributions with an average bond distance of 2.07 ± 0.03 Å, and one Co−S contribution at 2.26 ± 0.02 Å (Table 2, fit 7). Any attempt to resolve the Co−O/N distances failed, because of a high correlation in the ΔR parameters in the fit. Fitting of Co-TbADH to tetrahedral models was unstable and resulted in higher Debye−Waller and χ^2 values (Table 2, fits 1 and 2). The degree of stability in the fits was determined by reproducing the best distance and thermal disorder parameters using a wide range of initial conditions (e.g., bond distances ΔR). This procedure may indicate if the derived solution resides in a local minimum. Fits of Co-TbADH data to pentacoordination models (Table 2, fits 3−5) were stable only within narrow range of initial conditions ($-0.05 < \Delta R < 0.1$) in comparison to the fits of octahedral models ($-0.3 < \Delta R < 0.25$). Our final assignment of octahedral coordination is also supported by the lack of a 1s−3d pre-edge transition (see Figure 1).

The comparison of average Co−N and Co−O bond lengths in octahedral structures in the Cambridge Structural Database, including more than 2500 structures for each bond, reveals a similar distribution of bond distances of 2.00 ± 0.10 Å. Comparison of cobalt ligand bond distances in octahedral protein structures on the Metalloprotein Database at the Scripps Research Institute (http://metallo.scripps.edu) reveals that the average Co−Asp distance of 2.12 ± 0.15 Å (derived from 132 structures) and the average Co−Glu distance of 2.15 ± 0.12 Å (derived from 92 structures), and the Co−H$_2$O distance of 2.17 ± 0.22 Å (derived from 138 structures) tend to be slightly shorter than the Co−His distance of 2.25 ± 0.14 Å (derived from 47 structures). Yet we found that we cannot assign our EXAFS distance solution to specific ligands on the basis of this database search.

The EXAFS curve fitting analysis was complemented by bond valence sum (BVS) analysis. BVS is used to assess the compatibility of a given set of metal−ligand bond lengths with the assignment of a particular oxidation state to a central metal atom in a coordination complex. The calculations are based on the concept that the valence of the *j*th metal atom or ion, z_j, can be defined (eq 3) in terms of the sum of individual bond valences, V_{ij}.

$$z_j = \sum V_{ij} \qquad (3)$$

The bond valences (*s*) are calculated using the relationship

Table 2: EXAFS Curve Fitting Parameters[a]

fit	sample	χ^2	M–N/O ΔE_0	N	R (Å)	σ^2	M–N/O ΔE_0	N	R (Å)	σ^2	M–S ΔE_0	N	R (Å)	σ^2	M–C ΔE_0	N	R (Å)	σ^2	BVS[c]
	Zn-TbADH[b]		0 (F)	1 (F)	1.81(3)	1.6×10^{-5}	0.0 (F)	2 (F)	2.00(2)	3.5×10^{-3}	0 (F)	1 (F)	2.24(1)	1.0×10^{-6}					2.2–2.3
	Zn-TbADH complex[b]		−2.7 (F)	2 (F)	1.83(3)	1.6×10^{-5}	−2.7 (F)	2 (F)	2.05(3)	1.4×10^{-3}	−2.7 (F)	1 (F)	2.25 (F)	1.0×10^{-4}					2.7–2.8
1	Co-TbADH (4:3−1)	89	−4.4 (F)	3 (F)	2.03(1)	4.6×10^{-3}					−4.4 (F)	1 (F)	2.31(1)	2.2×10^{-3}	−2 (F)	3 (F)	2.93(1)	3.3×10^{-3}	2.0
2	Co-TbADH (4:1−2−1)	156	−4.9 (F)	1 (F)	1.96(14)	4.3×10^{-3}	−4.9 (F)	2 (F)	2.05 (11)	1.0×10^{-7}	−4.9 (F)	1 (F)	2.32(4)	2.5×10^{-3}	0.8 (F)	3 (F)	2.99 (F)	2.4×10^{-3}	2.0–2.1
3	Co-TbADH (5:4−1)[d]	67	−4.0 (F)	4 (F)	2.05(1)	9.1×10^{-3}					−4.0 (F)	1 (F)	2.29(1)	3.0×10^{-3}	−1.0 (F)	3 (F)	2.94(1)	3.7×10^{-3}	2.4
4	Co-TbADH (5:1−3−1)[e]	65	−4.1 (F)	1 (F)	1.92(4)	3.7×10^{-4}	−4.1 (F)	3 (F)	2.08 (2)	2.0×10^{-5}	−4.1 (F)	1 (F)	2.30(4)	9.0×10^{-3}	0.8 (F)	3 (F)	2.99 (F)	3.9×10^{-3}	2.4–2.5
5	Co-TbADH (5:2−2−1)[f]	75	−4.1 (F)	2 (F)	1.98(4)	6.4×10^{-3}	−4.1 (F)	2 (F)	2.09 (5)	1.0×10^{-7}	−4.1 (F)	1 (F)	2.30(4)	7.7×10^{-3}	0.8 (F)	3 (F)	2.99 (F)	3.6×10^{-3}	2.5
6	Co-TbADH (6:5−1)	60	−3.4 (F)	5 (F)	2.08(1)	1.3×10^{-2}					−3.4 (F)	1 (F)	2.27(1)	3.0×10^{-3}	0.6 (F)	3 (F)	2.94(1)	3.7×10^{-3}	2.7
7	Co-TbADH (6:1−4−1)	64	−5.5 (F)	1 (F)	1.86(3)	3.0×10^{-3}	−5.5 (F)	4 (F)	2.07 (2)	3.2×10^{-3}	−5.5 (F)	1 (F)	2.26(5)	5.0×10^{-3}	1.6 (F)	3 (F)	2.99 (F)	5.0×10^{-3}	3.0–3.1
8	Co-TbADH (6:2−3−1)	65	−5.5 (F)	2 (F)	1.95(4)	1.1×10^{-2}	−5.5 (F)	3 (F)	2.09 (2)	4.0×10^{-3}	−5.5 (F)	1 (F)	2.26(4)	4.6×10^{-3}	1.6 (F)	3 (F)	2.99 (F)	5.0×10^{-3}	3.0
9	Co-TbADH (guess)	66	−5.5 (F)	1 (F)	1.88 (F)	5.3×10^{-3}	−5.5 (F)	4.0(4)	2.07 (F)	5.0×10^{-3}	−5.5 (F)	1 (F)	2.26 (F)	5.0×10^{-3}	1.6 (F)	3 (F)	2.99 (F)	5.8×10^{-3}	3.0–3.1
10	Co-TbADH complex (4:3−1)	249	−1.0 (F)	3 (F)	2.07(1)	2.9×10^{-3}					−1.0 (F)	1 (F)	2.35 (F)	1.6×10^{-2}	3.4 (F)	3 (F)	3.02(1)	5.5×10^{-3}	1.8
11	Co-TbADH-complex (4:1−2−1)	230	−1.0 (F)	1 (F)	2.00(20)	1.2×10^{-3}	−1.0 (F)	2 (F)	2.10 (8)	1.0×10^{-7}	−1.0 (F)	1 (F)	2.32 (F)	1.7×10^{-2}	3.4 (F)	3 (F)	3.02(4)	5.6×10^{-3}	2.0
12	Co-TbADH complex (5:4−1)	140	−1.0 (F)	4 (F)	2.09(1)	6.8×10^{-3}					−1.0 (F)	1 (F)	2.26 (F)	9.4×10^{-3}	3.4 (F)	3 (F)	3.01(2)	6.4×10^{-3}	2.3
13	Co-TbADH complex (5:1−3−1)	133	−1.0 (F)	1 (F)	2.00(20)	3.4×10^{-3}	−1.0 (F)	3 (F)	2.12 (9)	2.0×10^{-5}	−1.0 (F)	1 (F)	2.25 (F)	1.1×10^{-2}	3.4 (F))	3 (F)	3.01(3)	6.8×10^{-3}	2.3
14	Co-TbADH complex (6:5−1)	81	−1.0 (F)	5 (F)	2.11(1)	1.2×10^{-2}					−1.0 (F)	1 (F)	2.27 (F)	3.1×10^{-3}	3.4 (F)	3 (F)	3.00(2)	7.8×10^{-3}	2.5
15	Co-TbADH complex (6:1−4−1)	67	−1.0 (F)	1 (F)	1.95(3)	1.4×10^{-3}	−1.0 (F)	4 (F)	2.14 (2)	3.2×10^{-3}	−1.0 (F)	1 (F)	2.24 (F)	1.5×10^{-3}	3.4 (F)	3 (F)	3.00(2)	8.9×10^{-3}	2.7
16	Co-TbADH complex (6:2−3−1)	68	−1.0 (F)	2 (F)	2.00(4)	4.8×10^{-3}	−1.0 (F)	3 (F)	2.17 (2)	4.0×10^{-3}	−1.0 (F)	1 (F)	2.24 (F)	1.1×10^{-3}	3.4 (F)	3 (F)	3.00(2)	8.9×10^{-3}	2.8–2.9
17	Co-TbADH complex (guess)	67	−1.0 (F)	1 (F)	2.00(5)	1.6×10^{-3}	−1.0 (F)	4.0(4)	2.15 (F)	5.0×10^{-3}	−1.0 (F)	1 (F)	2.24 (F)	1.4×10^{-3}	3.4 (F)	3 (F)	3.00 (F)	8.9×10^{-3}	2.5–2.6

[a] Results of EXAFS curve fitting analysis for Co-TbADH (fits 1−9) and of Co-TbADH in a complex with NADP^{+} and DMSO (fits 10−17). F stands for fixed and indicates that the parameter was fixed in the fit model. R is the distance of atoms from the metal ion (M) in angstroms. N is the number of atoms. σ^2 is the Debye−Waller factor. ΔE_0 is the correction to the energy origin. Fixing of a specific parameter was executed only after varying it and choosing its best value. The uncertainties regarding the R parameter are shown in parentheses. [b] The fitting results for Zn-TbADH and Zn-TbADH in complex with NADP^{+} and DMSO are from ref *15*. [c] BVS analysis was preformed using published values for each metal−ligand combination obtained from ref *43*. [d] Stable only for initial conditions under which the M−N/O I distance equals 2.00−2.15 Å. [e] Stable only for initial conditions under which the M−N/O I distance equals 1.85−2.00 Å and the M−N/O II distance equals 2.00−2.15 Å. [f] Stable only for initial conditions under which the M−N/O I distance equals 1.90−2.16 Å and the M−N/O II distance equals 2.04−2.17 Å.
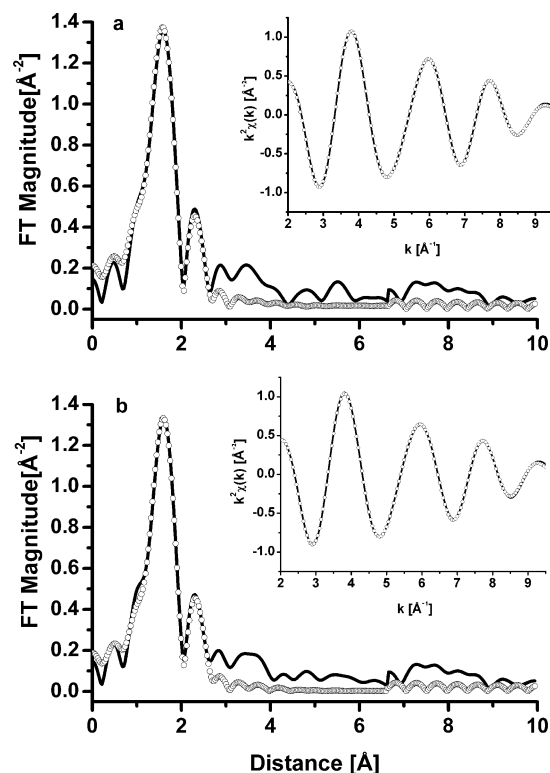
FIGURE 2: EXAFS curve fitting analysis of (a) apo-Co-TbADH and (b) the Co-TbADH−NADP$^+$−DMSO ternary complex to simulated theoretical zinc ligand contributions of the TbADH active site. The solid line indicates the experimental data, and the empty circles represent the best fits. Insers show the best fits in back-transformed representation. Experimental data were extracted and normalized using the UWXAFS analysis package. The theoretical XAFS signal was constructed of apo-CbADH subunit B active site data (PDB entry 1PED) (*14*) or aqua-thiourea[(*N,N*-diacetato)-semicarbazido-*N,O,O′,O″*]cobalt(II) (*30*) as a model calculated using FEFF7 (*28, 29*). The fitting analysis procedure is described in the text. The quality of the fits and parameters are presented in Table 2.

for a valence (V_i) of a given bond

$$V_i = \exp[(r_0 - r)/B] \qquad (4)$$

where B is a constant (0.37 Å), r is the length of a given bond, and r_0 is an empirical parameter for a given metal−ligand combination obtained either from published tables or from standard equations (*43−46*). The BVS value is generally close to the formal oxidation state of the metal. This type of analysis is useful for interpreting EXAFS data of metalloproteins, where the bond lengths are determined with a high precision (*46*). The complementary BVS values obtained for each fit of Co-TbADH are listed in Table 2. The BVS calculation of the best fit of Co-TbADH is in the range of 3.0−3.1. These values are higher than those obtained for Zn-TbADH (2.2−2.3), indicating that the change to a higher coordination number for Co-TbADH is followed by the accumulation of an additional positive charge on the catalytic metal ion.

The EXAFS analysis of the inhibited complex, Co-TbADH−NADP$^+$−DMSO (holo-Co-TbADH−DMSO), was best fitted with six Co−O/N ligands: one Co−O/N ligand at 1.95 ± 0.03 Å, four Co−O/N ligands at 2.14 ± 0.02 Å, and one Co−S ligand at 2.24 ± 0.02 Å (Table 2, fit 16). All attempts to constrain the fit to four or five ligands resulted

in unacceptable Debye−Waller factors (>0.01 for first-shell coordination), large uncertainties in the distance parameters, and high χ^2 values (fits 10−14). These results show that the binding of DMSO did not change the coordination number of the catalytic cobalt of Co-TbADH in its ternary complex, which remained six-coordinate, as observed for Co-TbADH alone. The similar geometry of the cobalt ion in both complexes and their calculated BVS values are in agreement with the absence of the edge shift seen in our edge analysis (Figure 1b).

Overall, our XAS analysis indicates structural differences between Zn-TbADH and Co-TbADH. These changes resulted in a different total effective charge and coordination of the catalytic metal. Yet Co-TbADH and Zn-TbADH have similar far-UV circular dichroism spectra (*1*). Therefore, we propose that the cobalt substitution induces only local structural changes at the catalytic metal site. Similar local changes in metal bond distances and coordination upon zinc to cobalt substitution have been observed before for other metalloenzymes (*40, 47−49*). In fact, zinc and cobalt γ-class carbonic anhydrase from *Methanosarcina thermophila* have almost identical three-dimensional structures (*48*). However, in these enzymes, the zinc is pentacoordinate to three histidine residues and two water molecules. Interestingly, the cobalt ion in the substituted enzyme is coordinated to an additional water molecule, thus forming a hexacoordinate complex with enhanced activity (*48, 50*). The expanded coordination of this cobalt-substituted γ-class carbonic anhydrase enzyme was suggested to enhance the reaction rates by a ligand stabilization process occurring because of the additional ligand binding to the catalytic metal (*48*). Similarly, thermolysin exhibits a 2-fold increase in its activity toward some substrates upon substitution of the zinc ion for cobalt while increasing the coordination number of the metal ion from four to five (*47*). The change in the metal coordination number is derived from the ligation of two water molecules to the metal site, rather than one in zinc-bound thermolysin. Interestingly, the water molecules coordinate the cobalt ion in positions that superimpose the proposed positions of the substrate carbonyl oxygens in the five-coordinated transition state (*47*).

The binding of DMSO to Co-TbADH did not change the coordination number of the catalytic site (Table 2), yet the coordination of DMSO to the cobalt ion in the substituted enzyme induced a small variation in the bond distance, which may result in minor conformational changes within the enzyme active site for accommodation of the substrate and place it in a favorable position for catalysis. In this respect, the higher coordination detected for the cobalt ion in substituted TbADH facilitates a more reactive catalytic site by stabilizing an intermediate-state structure, which may evolve during catalysis, as was suggested for cobalt-substituted thermolysin (*47*).

Interestingly, substitution of the TbADH catalytic zinc ion for manganese has shown to cause a 2.4-fold enhancement of the enzymatic activity (compare to the 1.4-fold enhancement caused by cobalt) (*1*). Manganese tends to bind proteins in an octahedral arrangement, whereas for zinc, a tetrahedral geometry is preferred (*51, 52*). Our preliminary XAS results with the manganese-substituted TbADH show the unique characteristics of octahedral coordination (data not shown). These results further demonstrate the linkage between the

metal coordination state and the reaction rates in TbADH.

DFT/B3LYP Calculations. To provide further insights into the energetic profile, complex geometry, and origin of the two Co−O contributions detected by our XAS analysis, we carried out a series of quantum chemical calculations. Initially, our model systems consisted of metal ions, Co^{2+} and Zn^{2+}, and the side chains of amino acid residues that directly participate in metal−ligand bonds: Asp, Glu, Cys, and His. The former three were considered in their deprotonated forms (i.e., as carboxylates and methylthiolate). The starting geometries were taken from the available three-dimensional structure of TbADH (*14*) and optimized (data not shown). The gas-phase complexation energies of both ions, computed at the B3LYP/6-311++G(2df,2pd) level, using eq 2, are −600.4 kcal/mol for cobalt(II) and −598.4 kcal/mol for zinc(II). These results indicate that both Co^{2+} and Zn^{2+} have a tendency to form tetrahedral complexes using the first-coordination shell residues of the metal ion in TbADH.

In the next step, the hypothesis, whether the additional two Co−O contributions detected at the metal ion in Co-TbADH result from the binding of two water molecules, thus causing a transition into an octahedral geometry, was tested. The starting structures were built up from the four-coordinated models calculated in the previous steps with the four L−M−L angles changed from the "tetrahedral" (approximately 109°) to "octahedral" values (approximately 90°) and the two empty positions occupied by two water molecules. Surprisingly, the optimization of the gas-phase model resulted in the tetrahedral structure of the binding site (for both ions) with the water molecules being expelled into the second solvation sphere (data not shown). The complexation energies, recalculated at the B3LYP/6-311++G(2df,2pd) level, using eq 2, are −517.4 kcal/mol for cobalt(II) and −525.0 kcal/mol for zinc(II). These values correspond to the reaction energy for the following reaction:

$$[M(H_2O)_6]^{2+} + \{(His)(Asp)(Glu)(Cys)(H_2O)_2\} \rightarrow$$
$$\{(H_2O)_6\} + [M(His)(Asp)(Glu)(Cys)(H_2O)_2]^{2+}$$
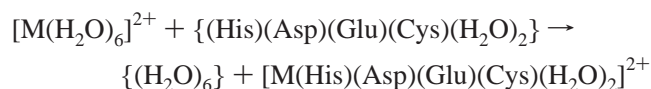
where {(A)(B)...} denotes the cluster of ligands preorganized in the equilibrium geometry of the [M(A)(B)...]²⁺ complex. Overall, these results suggest that Co^{2+} has no significant preference to form hexacoordinate complexes over Zn^{2+} in the contents of the TbADH active site.

Further attempts to obtain stable hexacoordinate Co^{2+} were made using the carboxylate groups of Asp and Glu as potential bidentate metal-coordinating ligands. These groups may bind metals in several modes: *syn*, *anti*, and bidentate (the binding *syn* mode is characterized by the metal−O−C−O torsion angle of bound carboxylate approaching 0°, whereas it is ∼180° for the *anti* mode). The existence of the bidentate binding mode can possibly account for the presence of six atoms in the first coordination sphere in Co-TbADH. The geometry optimizations of four conformers, combinations of *syn* and *anti* binding modes, of model [M(HCOO)₂(CH₃S)(CH₃NCH₂)]⁻ complexes have been carried out (data not shown). The molecular energies of all four studied conformers are listed in Table 3. The optimizations of the molecular geometries of conformers with a purely bidentate binding mode of carboxylates have not yielded the

Table 3: Molecular Energy Values[a]

	syn,syn	*syn,anti*	*anti,syn*	*anti,anti*
Co^{2+}	2.2	0.0	3.8	2.5
Zn^{2+}	1.8	0.0	3.3	2.6

[a] The molecular energies of various conformers of the [M(HCOO)₂(CH₃S)(CH₃NCH₂)]⁻ system used as the model for the investigation of the possible binding modes of carboxylates at the site in ADH. All values are in kilocalories per mole.
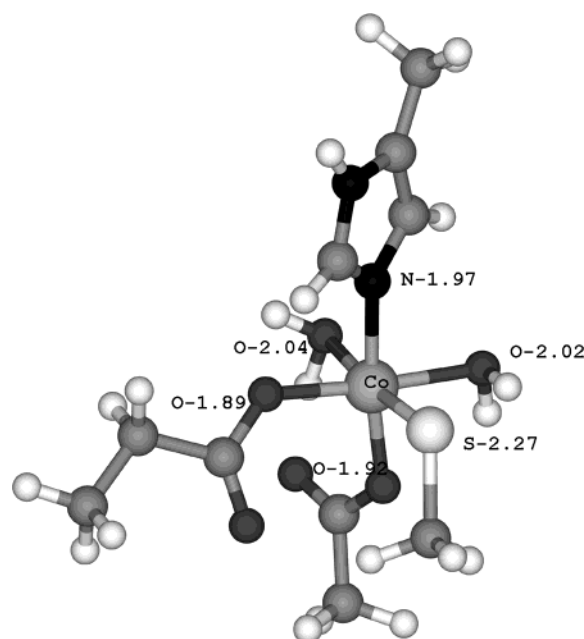

FIGURE 3: Equilibrium geometry of a model cobalt(III) complex mimicking the metal-binding site of alcohol dehydrogenase [Co-(His)(Asp)(Glu)(Cys)(H₂O)₂]. Metal−ligand distances are in angstroms.

minima on the potential energy surface. Instead, the optimizations ended up in the nearest *syn,syn* mode. Therefore, in agreement with the results previously described, the calculations do not suggest any significant tendency of Co^{2+} (relative to Zn^{2+}) to form hexacoordinate complexes using the mode of binding made available by the carboxylate residues. These results are in good agreement with our previous observations (*16*) and the XAS and BVS analyses reported here, indicating that the formation of higher-coordination complexes with both Zn-TbADH and Co-TbADH utilizes the accumulation of partial positive charge on the metal ion.

In agreement with this statement, the quantum chemical calculations of the model complex [Co³⁺(Asp⁻)(Glu⁻)(His)(Cys⁻)(H₂O)₂] have been carried out [the Co³⁺ has been considered in its closed shell singlet state, i.e., $(t_{2g})^6(e_g)^0$ electron configuration]. The obtained equilibrium (optimized) geometry clearly shows that the studied complex is stable using octahedral coordination geometry. This can be explained by the much stronger electrostatic interaction between the formally (3+) charged metal ion and the negatively charged ligands. The equilibrium structure and metal−ligand distances are depicted in Figure 3. The metal−ligand distances obtained by EXAFS analysis are in good agreement with the corresponding calculated values. The Co−S(Cys) distance of 2.26 ± 0.02 Å obtained by EXAFS is in excellent agreement with the calculated value of 2.27 Å. The EXAFS results of one Co−N/O bond at 1.86 ± 0.03 Å may

correspond to a Co−Asp distance of 1.92 Å or a Co−Glu distance of 1.89 Å. The former alternative may be more likely, since the binding of Glu-60 is considered to be weaker due to the steric constraints exercised by the rest of the protein. Therefore, we assume that four clustered Co−O/N distances (2.07 ± 0.03 Å) can be assigned to Co−N(His) bonds of 1.97 Å, Co−O(H_2O) bonds of 2.02 and 2.04 Å, and the previously discussed Co−O(Glu-60) distance. The nearest environment (energy-minimized) of the cobalt ion in Co-TbADH shown in Figure 3 describes a symmetric octahedral Co−ligand complex where two additional water molecules coordinate the metal ion. The high level of symmetry suggested in Figure 3 is also supported by our edge analysis (see Figure 1). Nevertheless, in this stage we cannot exclude the possibility that other active site ligands may coordinate to the metal ion via oxygen and/or nitrogen ligation instead of water.

An important aspect of metalloenzyme catalysis is the electronic and charge changes (*53*, *54*). The DFT calculations presented here suggest that the Co^{2+} ion undergoes oxidation while forming an octahedral structure complex at the Co-TbADH catalytic site. The higher valence of the cobalt ion in Co-TbADH is supported by our BVS analysis (Table 2). Interestingly, binding of DMSO to the Zn-TbADH active site induced a distinct change in the metal charge, as observed by XANES (*15*) and BVS calculations (Table 2), whereas in Co-TbADH, the binding of DMSO did not cause such changes (Figure 1 and Table 2). A possible explanation for these results may lie in the different Lewis acidity properties of the cobalt and zinc ions (*17*). Importantly, our previously reported time-resolved XAFS studies of TbADH catalysis provide real-time experimental evidence of the dynamic perturbation of the metal ion valence during substrate turnover (*16*). The change in the total effective charge of the zinc ion indicates a continuous biphasic process consisting of an initial rapid linear phase of building up a partial positive charge on the metal ion, followed by an opposing slow exponential phase, which neutralizes the charge. The accumulation of a partial positive charge on the catalytic zinc ion correlates with the assembly of pentacoordinated intermediates (*16*). Therefore, the higher valence of the catalytic metal in Co-TbADH reported here may contribute to and facilitate substrate binding and stabilization of the reaction intermediates.

A different kinetic behavior occurring upon cobalt substitution of enzymes from the same enzymatic family was observed for the γ-class carbonic anhydrases, where cobalt substitution doubled the activity of bacterial thermophilic γ-class carbonic anhydrase and reduced the activity of human carbonic anhydrase isozyme (*48*, *50*). Cobalt-substituted thermolysine exhibited >2-fold more activity than zinc thermolysine (*55*, *56*). Astacin exhibits an ~1.4-fold increased activity upon cobalt substitution (*57*), whereas such a substitution of astacin-like *Serratia* metalloendopeptidase catalytic zinc caused a >2000% increase in activity (*58*). It has been proposed that the enhanced activity is caused by the metal substitution of these enzymes, which initiated a structural change in the metal coordination sphere, which seems to provide a low-energy pathway that is needed for the reaction to take place (*50*, *58*).

CONCLUSIONS

In the study presented here, a cobalt substitution was utilized to assign the reaction mechanism of TbADH. Specifically, by using kinetics, X-ray absorption, and DFT calculations, we characterized the local structure and electronics of the active site of Co-TbADH. Co-TbADH exhibits enhanced activity and a different local structure around the catalytic metal ion compared with Zn-TbADH. XAS analysis of Co-TbADH reveals that the metal ion possesses octahedral coordination and not tetrahedral coordination as in Zn-TbADH; binding of DMSO to Co-TbADH is by substitution of another ligand while octahedral coordination is maintained and not by coordination expansion, as seen with Zn-TbADH (*15*, *59*). BVS analysis and DFT calculations suggest that these local structural changes of Co-TbADH are accompanied by the partial oxidation of the catalytic metal ion (*15*, *16*). Taken together, the work presented here addresses the important role of the metal in metalloenzyme catalysis and demonstrates the tight connection between enzymatic activity, metal charge, and the coordination state.

REFERENCES

1. Bogin, O., Peretz, M., and Burstein, Y. (1997) *Thermoanaerobacter brockii* alcohol dehydrogenase: characterization of the active site metal and its ligand amino acids, *Protein Sci. 6*, 450−458.
2. Sun, H. W., and Plapp, B. V. (1992) Progressive sequence alignment and molecular evolution of the Zn-containing alcohol dehydrogenase family, *J. Mol. Evol. 34*, 522−535.
3. Galdes, A., and Vallee, B. L. (1983) in *Metal ions in biological systems* (Sigel, H., Ed.) pp 1−54, Dekker, New York.
4. Zeppezauer, M. (1983) Coordination properties and mechanistic aspects of liver alcohol dehydrogenase, *NATO Adv. Study Inst. Ser., Ser. C 100*, 99−122.
5. Wilkinson, G. (1987) *Comprehensive Coordination Chemistry: The Synthesis, Reactiones, Properties and Applications of Coordination Compounds*, Vol. 5, Pergamon Press, London.
6. Bertini, I., Luchinat, C., Maret, W., and Zeppezauer, M. (1986) *Zinc Enzymes*, Vol. 1, Birkhauser, Boston.
7. Dunn, M. F., Biellmann, J. F., and Branlant, G. (1975) Roles of zinc ion and reduced coenzyme in horse liver alcohol dehydrogenase catalysis. The mechanism of aldehyde activation, *Biochemistry 14*, 3176−3182.
8. Eklund, H., Plapp, B. V., Samama, J. P., and Branden, C. I. (1982) Binding of substrate in a ternary complex of horse liver alcohol dehydrogenase, *J. Biol. Chem. 257*, 14349−14358.
9. Dworschack, R. T., and Plapp, B. V. (1977) Kinetics of native and activated isozymes of horse liver alcohol dehydrogenase, *Biochemistry 16*, 111−116.
10. Makinen, M. W., Maret, W., and Yim, M. B. (1983) Neutral metal-bound water is the base catalyst in liver alcohol dehydrogenase, *Proc. Natl. Acad. Sci. U.S.A. 80*, 2584−2588.
11. Lamed, R. J., and Zeikus, J. G. (1981) Novel NADP-linked alcohol−aldehyde/ketone oxidoreductase in thermophilic ethanologenic bacteria, *Biochem. J. 195*, 183−190.
12. Lamed, R., and Zeikus, J. G. (1980) Ethanol production by thermophilic bacteria: relationship between fermentation product yields of and catabolic enzyme activities in *Clostridium thermocellum* and *Thermoanaerobium brockii*, *J. Bacteriol. 144*, 569−578.
13. Peretz, M., and Burstein, Y. (1989) Amino acid sequence of alcohol dehydrogenase from the thermophilic bacterium *Thermoanaerobium brockii*, *Biochemistry 28*, 6810−6815.
14. Korkhin, Y., Kalb, A. J., Peretz, M., Bogin, O., Burstein, Y., and Frolow, F. (1998) NADP-dependent bacterial alcohol dehydro-

genases: crystal structure, cofactor-binding and cofactor specificity of the ADHs of *Clostridium beijerinckii* and *Thermoanaerobacter brockii*, *J. Mol. Biol. 278*, 967−981.

15. Kleifeld, O., Frenkel, A., Bogin, O., Eisenstein, M., Brumfeld, V., Burstein, Y., and Sagi, I. (2000) Spectroscopic studies of inhibited alcohol dehydrogenase from *Thermoanaerobacter brockii*: proposed structure for the catalytic intermediate state, *Biochemistry 39*, 7702−7711.

16. Kleifeld, O., Frenkel, A., Martin, J. M., and Sagi, I. (2003) Active site electronic structure and dynamics during metalloenzyme catalysis, *Nat. Struct. Biol. 10* (2), 98−103.

17. Maret, W., and Vallee, B. L. (1993) Cobalt as probe and label of proteins, *Methods Enzymol. 226*, 52−71.

18. Adolph, H. W., Maurer, P., Schneider-Bernlohr, H., Sartorius, C., and Zeppezauer, M. (1991) Substrate specificity and stereoselectivity of horse liver alcohol dehydrogenase. Kinetic evaluation of binding and activation parameters controlling the catalytic cycles of unbranched, acyclic secondary alcohols and ketones as substrates of the native and active-site-specific Co(II)-substituted enzyme, *Eur. J. Biochem. 201*, 615−625.

19. Schneider, G., Eklund, H., Cedergren-Zeppezauer, E., and Zeppezauer, M. (1983) Crystal structures of the active site in specifically metal-depleted and cobalt-substituted horse liver alcohol dehydrogenase derivatives, *Proc. Natl. Acad. Sci. U.S.A. 80*, 5289−5293.

20. Vanni, A., Pessione, E., Anfossi, C., Baggiani, C., Cavaletto, M., Gulmini, M., and Giunta, C. (2000) Properties of cobalt-reactivated form of yeast alcohol dehydrogenase, *J. Mol. Catal. B: Enzym. 9*, 283−291.

21. Maret, W., Andersson, I., Dietrich, H., Schneider-Bernlohr, H., Einarsson, R., and Zeppezauer, M. (1979) Site-specific substituted cobalt(II) horse liver alcohol dehydrogenases. Preparation and characterization in solution, crystalline and immobilized state, *Eur. J. Biochem. 98*, 501−512.

22. Dunn, M. F., Dietrich, H., MacGibbon, A. K., Koerber, S. C., and Zeppezauer, M. (1982) Investigation of intermediates and transition states in the catalytic mechanisms of active site substituted cobalt(II), nickel(II), zinc(II), and cadmium(II) horse liver alcohol dehydrogenase, *Biochemistry 21*, 354−363.

23. Maret, W. (1989) Cobalt(II)-substituted class III alcohol and sorbitol dehydrogenases from human liver, *Biochemistry 28*, 9944−9949.

24. Maret, W., and Makinen, M. W. (1991) The pH variation of steady-state kinetic parameters of site-specific Co^{2+}-reconstituted liver alcohol dehydrogenase. A mechanistic probe for the assignment of metal-linked ionizations, *J. Biol. Chem. 266*, 20636−20644.

25. Bradford, M. M. (1976) A rapid and sensitive method for the quantitation of microgram quantities of protein utilizing the principle of protein-dye binding, *Anal. Biochem. 72*, 248−254.

26. Roe, A. L., Schneider, D. J., Mayer, R. J., Pyrz, J. W., Widom, J., and Que, L., Jr. (1984) X-ray Absorption Spectroscopy of Iron-Tyrosinate Proteins, *J. Am. Chem. Soc. 106*, 1676−1681.

27. Stern, E. A., Newville, M., Ravel, B., Yacoby, Y., and Haskel, D. (1995) The UWXAFS analysis package: philosophy and details, *Physica B 208−209*, 117−120.

28. Zabinsky, S. I., Rehr, J. J., Ankudinov, A., Albers, R. C., and Eller, M. J. (1995) Multiple Scattering Calculations of X-ray Absorption Spectra, *Phys. Rev. B 52*, 2995−3009.

29. Rehr, J. J., Mustre de Leon, J., Zabinsky, S. I., and Albers, R. C. (1991) Theoretical X-ray absorption fine structure standards, *J. Am. Chem. Soc. 113*, 5135−5140.

30. Burshtein, I. F., Gerbeleu, N. V., Bannova, I. I., Bologa, O. A., Lozan, V. I., and Malinovskii, T. I. (1987) Crystalline-Structure of Cobalt(II) Aquothiocarbamidesemicarbazidediacetate, *Koord. Khim. 13*, 1690−1694.

31. Stern, E. A. (1993) Number of relevant independent points in X-ray-absorption fine-structure spectra, *Phys. Rev. B 48*, 9825−9827.

32. Frisch, M. J., Trucks, G. W., Schlegel, H. B., Scuseria, G. E., Robb, M. A., Cheeseman, J. R., Zakrzewski, V. G., Montgomery, J. A. J., Stratmann, R. E., Burant, J. C., Dapprich, S., Millam, J. M., Daniels, A. D., Kudin, K. N., Strain, M. C., Farkas, O., Tomasi, J., Barone, V., Cossi, M., Cammi, R., Mennucci, B., Pomelli, C., Adamo, C., Clifford, S., Ochterski, J., Petersson, G. A., Ayala, P. Y., Cui, Q., Morokuma, K., Malick, D. K., Rabuck, A. D., Raghavachari, K., Foresman, J. B., Cioslowski, J., Ortiz, J. V., Stefanov, B. B., Liu, G., Liashenko, A., Piskorz, P., Komaromi, I., Gomperts, R., Martin, R. L., Fox, D. J., Keith, T., Al-Laham, M. A., Peng, C. Y., Nanayakkara, A., Gonzalez, C.,

Challacombe, M., Gill, P. M. W., Johnson, B., Chen, W., Wong, M. W., Andres, J. L., Gonzalez, C., Head-Gordon, M., Replogle, E. S., and Pople, J. A. (1998) *Gaussian 98*, Gaussian, Inc., Pittsburgh, PA.

33. Becke, A. D. (1988) Density-functional exchange-energy approximation with correct asymptotic behavior, *Phys. Rev. A 38*, 3098−3100.

34. Wachters, A. J. H. (1970) Gaussian basis set for molecular wavefunctions containing third-row atoms, *J. Chem. Phys. 52*, 1033−1036.

35. Hay, P. J. (1977) Gaussian basis sets for molecular calculations. The representation of 3d orbitals in transition-metal atoms, *J. Chem. Phys. 66*, 4377−4384.

36. Krishnan, R., Binkley, J. S., Seeger, R., and Pople, J. A. (1980) Self-consistent molecular orbital methods. XX. A basis set for correlated wave functions, *J. Chem. Phys. 72*, 650−654.

37. Cotton, F. A., and Wilkinson, G. (1988) *Advanced inorganic chemistry*, 5th ed., Wiley, New York.

38. Rulisek, L., and Havlas, Z. (2000) Theoretical Studies of Metal Ion Selectivity. 1. DFT Calculations of Interaction Energies of Amino Acid Side Chains with Selected Transition Metal Ions (Co^{2+}, Ni^{2+}, Cu^{2+}, Zn^{2+}, Cd^{2+}, and Hg^{2+}), *J. Am. Chem. Soc. 122*, 10428−10439.

39. Wirt, M. D., Sagi, I., Chen, E., Frisbie, S. M., Lee, R., and Chance, M. R. (1991) Geometric Conformations of Intermediates of B12 Catalysis by X-Ray Edge Spectroscopy: Co(I) B12, Co(Ii) B12, and Base-Off Adenosylcobalamin, *J. Am. Chem. Soc. 113*, 5299−5304.

40. Yachandra, V., Powers, L., and Spiro, T. G. (1983) X-ray absorption spectra and the coordination number of Zn and Co carbonic anhydrase as a function of pH and inhibitor binding, *J. Am. Chem. Soc. 105*, 6596−6604.

41. Kruger, G. J., and Reynhardt, E. C. (1974) New investigation of the structure of trisacetylacetonatocobalt(III), *Acta Crystallogr. B30*, 822−824.

42. Al-Karadaghi, S., Cedergren-Zeppezauer, E. S., Hoevmoller, S., Petratos, K., Terry, H., and Wilson, K. S. (1994) Refined crystal structure of liver alcohol dehydrogenase-NADH complex at 1.8 Å resolution, *Acta Crystallogr. D50*, 793−807.

43. Brown, I. D., and Altermatt, D. (1985) Bond-Valence Parameters Obtained from a Systematic Analysis of the Inorganic Crystal Structure Database, *Acta Crystallogr. B41*, 244−247.

44. Liu, W., and Thorp, H. H. (1993) Bond Valence Sum Analysis of Metal−Ligand Bond Lengths in Metalloenzymes and Model Complexes. 2. Refined Distances and Other Enzymes, *Inorg. Chem. 32*, 4102−4105.

45. Wood, R. M., and Palenik, G. J. (1998) Bond valence sums in coordination chemistry. A simple method for calculating the oxidation state of cobalt in complexes containing only Co−O bonds, *Inorg. Chem. 37*, 4149−4151.

46. Thorp, H. H. (1998) Bond Valence Analysis of Metalloenzymes. 3. Predicting Bond Lengths in Adjacent Redox States Using Inner-Sphere Reorganizational Energies, *Inorg. Chem. 37*, 5690−5692.

47. Holland, D. R., Hausrath, A. C., Juers, D., and Matthews, B. W. (1995) Structural analysis of zinc substitutions in the active site of thermolysin, *Protein Sci. 4*, 1955−1965.

48. Iverson, T. M., Alber, B. E., Kisker, C., Ferry, J. G., and Rees, D. C. (2000) A closer look at the active site of γ-class carbonic anhydrases: high-resolution crystallographic studies of the carbonic anhydrase from *Methanosarcina thermophila*, *Biochemistry 39*, 9222−9231.

49. Brown, D. C., and Collins, K. D. (1991) Dihydroorotase from *Escherichia coli*. Substitution of Co(II) for the active site Zn(II), *J. Biol. Chem. 266*, 1597−1604.

50. Alber, B. E., Colangelo, C. M., Dong, J., Stalhandske, C. M., Baird, T. T., Tu, C., Fierke, C. A., Silverman, D. N., Scott, R. A., and Ferry, J. G. (1999) Kinetic and spectroscopic characterization of the γ-carbonic anhydrase from the methanoarchaeon *Methanosarcina thermophila*, *Biochemistry 38*, 13119−13128.

51. Bock, C. W., Katz, A. K., Markham, G. D., and Glusker, J. P. (1999) Manganese as a replacement for magnesium and zinc: Functional comparison of the divalent ions, *J. Am. Chem. Soc. 121*, 7360−7372.

52. Rulisek, L., and Vondrasek, J. (1998) Coordination geometries of selected transition metal ions (Co^{2+}, Ni^{2+}, Cu^{2+}, Zn^{2+}, Cd^{2+}, and Hg^{2+}) in metalloproteins, *J. Inorg. Biochem. 71*, 115−127.

53. Warshel, A., Strajbl, M., Villa, J., and Florian, J. (2000) Remarkable rate enhancement of orotidine 5′-monophosphate decarbox-

ylase is due to transition-state stabilization rather than to ground-state destabilization, *Biochemistry 39*, 14728−14738.

54. Ryde, U. (1995) On the role of Glu-68 in alcohol dehydrogenase, *Protein Sci. 4*, 1124−1132.

55. Kuzuya, K., and Inouye, K. (2001) Effects of cobalt-substitution of the active zinc ion in thermolysin on its activity and active-site microenvironment, *J. Biochem. 130*, 783−788.

56. Holmquist, B., and Vallee, B. L. (1974) Metal substitutions and inhibition of thermolysin: spectra of the cobalt enzyme, *J. Biol. Chem. 249*, 4601−4607.

57. Gomis-Ruth, F. X., Grams, F., Yiallouros, I., Nar, H., Kusthardt, U., Zwilling, R., Bode, W., and Stocker, W. (1994) Crystal structures, spectroscopic features, and catalytic properties of cobalt(II), copper(II), nickel(II), and mercury(II) derivatives of the zinc endopeptidase astacin. A correlation of structure and proteolytic activity, *J. Biol. Chem. 269*, 17111−17117.

58. Park, H. I., and Ming, L. J. (2002) Mechanistic studies of the astacin-like *Serratia* metalloendopeptidase serralysin: highly active (>2000%) Co(II) and Cu(II) derivatives for further corroboration of a "metallotriad" mechanism, *J. Biol. Inorg. Chem. 7*, 600−610.

59. Kleifeld, O., Frenkel, A., and Sagi, I. (2001) Time-dependent XAS studies of trapped enzyme−substrate complexes of alcohol dehydrogenase from *Thermoanaerobacter brockii*, *J. Synchrotron Radiat. 8*, 978−980.